Supporting Information

Zirconium Phosphate Catalyzed Transformations of Biomass Derived Furfural to Renewable Chemicals

Abhinav Kumar[a] and Rajendra Srivastava[a]*

[a]*Department of Chemistry, Indian Institute of Technology Ropar, Rupnagar, Punjab-140001, India*

---

*Corresponding Author Email: rajendra@iitrpr.ac.in

*Phone: +91-1881-242175; Fax: +91-1881-223395

This Supporting information has forty pages (S1-S40), and contains:

Four Supporting Schemes (Schemes S1-S4)

Fifteen Supporting Figures (Figures S1-S15)

Seven Supporting Tables (Tables S1-S7)

Materials

The Pluronic P123, hydrochloric acid (35 wt.%), zirconium propoxide (70 wt.% in 1-propanol), titanium isopropoxide (97%), furfural, furfural alcohol, 5-hydroxymethyl furfural (HMF), and ethanol were procured from Sigma Aldrich, Pvt. Ltd., India. H_3PO_4, solvents used in this study were purchased from Merck, Pvt. Ltd., India. $SnCl_2.2H_2O$, urea, and cyclohexanone were procured from Loba Chemie Pvt. Ltd., India. Acetophenone, cinnamaldehyde, benzaldehyde, acetylacetone, malononitrile, and 1-heptanal were obtained from Spectrochem. DFF was purchased from CDH Pvt. Ltd., India.

Catalyst Preparation

Synthesis of zirconium phosphate and titanium phosphate

Zirconium phosphate was synthesized by using P123 as a structure-directing agent.[R1] P123 (1 g) and 35 % HCl (0.2 g) was dissolved in 15 g ethanol for 30 min under ambient condition. To this solution, H_3PO_4 (10 mmol, 88 wt.%) was added and the reaction mixture was transferred in an ice bath followed by stirring for 2 h. Meanwhile, a solution containing zirconium propoxide (10 mmol) in 10 g ethanol was prepared and this solution was added to the above-mentioned reaction mixture and the resultant reaction mixture was stirred for 3 h at 273 K. The temperature of the reaction mixture was raised to ambient temperature. Then the obtained solid powder after solvent evaporation was calcined at 673 K for 6 h in air and the material is designated as $ZrPO_4$. Using the same synthesis recipe $TiPO_4$ was also prepared by using titanium isopropoxide as the titanium source.

Synthesis of crystalline $ZrPO_4$

The crystalline $ZrPO_4$ was synthesized according to the literature report.[R2] $ZrOCl_2.8H_2O$ (4.0 g) was added to 40 mL H_3PO_4 (3.0 M) aqueous solution under the stirring condition at ambient temperature for 3 h. The resultant mixture was hydrothermally treated in a Teflon-lined steel vessel at 473 K for 24 h. After cooling the autoclave to ambient temperature, the solid material was separated by centrifugation and washed with water until it becomes neutral. Finally, the solid material was dried at 373 K in an oven to obtain the crystalline $ZrPO_4$.

Synthesis of $SnPO_4$

Tin phosphate was synthesized by following the reported procedure.[R3] P123 (1 g) and H_3PO_4 (10 mmol) were dissolved in 15 g water in a polypropylene bottle and the mixture was stirred for 2 h at ambient temperature.$SnCl_2.2H_2O$ (10 mmol) was dissolved in 5 g water, and the solution was slowly added to the above mixture under the stirring condition and the stirring was continued for another 3 h. The obtained white gel was transferred in a Teflon-line autoclave and hydrothermally treated at 373 K for 72 h. The obtained white solid precipitate was separated by centrifugation, washed with distilled water and dried in an oven at 343 K for 12 h. The dried white powder was calcined at 773 K for 5 h to obtain $SnPO_4$.

Material Characterization

The materials were first characterized by an X-ray diffraction (XRD) technique using a RIGAKU Mini-flex diffractometer in 5-80^o 2θ range with Cu kα (λ = 0.154 nm) radiation. The porosity and surface area of the materials were determined usingN_2-sorption measurements on a Quantachrome Instrument, Autosorb-IQ, USA. Before the sorption analysis, samples were degassed at 473 K for 6 h in the degassing ports. A relative pressure range of 0.05 to 0.3 was selected to calculate the specific surface area of the catalyst usingBrunauer-Emmett-Teller (BET) equation. The pore size distribution was calculated from the desorption branch using Barrett-Joyner-Halenda (BJH) method. The morphological and microstructural properties were analyzed by Scanning Electron Microscopy (SEM) JEOL JSM-6610LV, and transmission electron microscope (TEM) 200KV (TALOS F200S G2) at CeNS, Bengaluru. The composition of various elements in the material was determined by energy-dispersive X-ray spectroscopy (EDX). The presence of various elements and their oxidation states were analyzed by X-Ray photoelectron spectroscopy (XPS) on a Thermofisher scientific (Nexsa base) instrument. The functional groups present in the materials were analyzed by the Fourier transform-Infra red (FT-IR) technique using a Bruker Tensor-II F-27 instrument associated with Pt-ATR assembly. The same FT-IR instrument was used for the estimation of different kinds of acid sites present in the materials by using pyridine as a probe molecule. The temperature-programmed desorption (TPD) techniques, NH_3-TPD and CO_2-TPD were used for total acidity and total basicity measurements, respectively on a Quantachrome, CHEMBET^{TM} TPR/TPD instrument. For the analysis, the samples were preheated at 573 K at a heating rate of 10 deg/min under a continuous He flows for 30 min. Then, the sample cell was cooled to 323 K, and the gas NH_3(10% in He) or CO_2 was adsorbed by flowing the gas for 1 h in the sample cell with the flow rate of 10 mL/min.

The excess or physically adsorbed gas was removed by He flow (50 mL/min) for 30 min. Finally, the amount of desorbed gas was monitored by a temperature-controlled device (TCD) as the function of temperature in the range of 350-1000 K with a ramp rate of 10 deg/min. The zeta potential measurement was performed on a ZETA-Check-Colloid Metrix instrument with 10 mL 2-propanol, 100 mg catalyst, and 1mmol substrate. The UV-visible adsorption was performed on a Shimadzu UV-2600 spectrophotometer instrument. For the adsorption study of furfural and benzaldehyde, 10 ppm 50 mL solution was prepared in n-hexane and 100 mg of the solid catalyst was used. However, for the cinnamaldehyde chloroform was chosen instead of n-hexane because of the insolubility of cinnamaldehyde in n-hexane.

Procedures of Catalytic Reactions

Catalytic transfer hydrogenation of furfural and other organic compounds

A 50 ml autoclave was charged with furfural (1 mmol), catalyst (50 mg), and 2-propanol (7 mL). To create an oxygen-free environment, the autoclave was purged with N_2 for three times and pressurized up to2 bar with N_2 gas. The time when the reaction temperature reached the desired temperature, was considered as the starting time of the reaction. After the desired time the reaction was stopped and the autoclave was allowed to cool naturally. Then catalyst was removed from the reaction mixture by centrifugation and analyzed by gas chromatography (GC) (Yonglin; 6100; GC column: BP-5; 30 m×0.25 mm×0.25μm) fitted with aFlame ionization detector (FID). High purity N_2 gas (99.99%, GC grade) was used as the carrier gas with a flow rate of 10 ml/min whereas H_2 (99.99%, GC grade) and Air (99.99%, GC grade) were used as ignition gases. The injector and detector temperature were set at 553 K. GC column oven temperature was programmed as follows: Initial temperature = 353 K, hold time = 2 min, followed by temperature ramping to a final temperature of 573 K with a ramp rate of 10 K/min. 0.4 μL of the sample was injected for the analysis. The product identification was carried out by using Gas chromatograph-Mass spectrometer (GC-MS) (Shimadzu GCMS-QP 2020 NX). The concentrations of FAL, FOL, and 2-(isopropoxymethyl)furan were calculated by standard addition method using calibration curves based on these compounds obtained from the commercial market. Similarly, the concentrations of HMF, DFF, and compounds represented as a to c in Table S4 were calculated by standard addition method using calibration curves based on these compounds obtained from the commercial market. Quantitative analysis of product d (Table S4) was

based on the calibration curve of other chemicals just discussed above. Mass balance was calculated by measuring the mass before and after the reaction. Mass balance was also verified by GC analysis based on the mass of the reactant conversion and masses of the products formed after the reaction. Carbon balance was calculated by the following equation: Carbon balance = (moles of product/moles of furfural converted) x 100.[R4]

Biginelli reaction

In a two neck round bottom flask, acetylacetone (1 mmol), aldehyde (1mmol), urea (1.5 mmol), and catalyst (50 mg) were charged. The flask was heated at 353 K under stirring for the desired time-period. Progress of the reaction was monitored by thin-layer chromatography (TLC) (using hexane and ethyl acetate as eluent). On completion of the reaction, 4 ml of distilled water was added to the reaction mixture and the solid product was filtered and washed with water to remove the excess of urea. The obtained Biginelli product was vacuum dried in a desiccator. The product was confirmed by ^{1}H and ^{13}C NMR (Jeol, 400 MHz) spectra recorded in DMSO-d^{6} that match well with the reported NMR data.

The obtained yellowish solid product along with catalyst was diluted with 4 mL of distilled water and it was stirred for some time to make a homogeneous solution. The Biginelli product obtained from HMF was completely soluble at room temperature in water. At this stage, the catalyst was removed from the reaction mixture by simple centrifugation. Then the product was precipitated by cooling it to 273 K in the refrigerator. The cold reaction mixture of the HMF derived product was filtered and the obtained precipitate was washed with 4 mL of cold water. The final obtained solid product was dried in a vacuum desiccator at ambient temperature for 48 h. However, in the case of FF and other aldehyde derived products, a precipitate was deposited at the bottom of the reaction flask after adding water into it. The precipitated products obtained from other aldehydes were filtered along with the catalyst in order to separate the solid precipitate. The obtained solid precipitate was then dissolved in hot ethanol and the catalyst was filtered using filter paper. The ethanol was evaporated using a rotary evaporator, followed by vacuum drying to obtain the Biginelli product.

Knovenangel condensation reaction

In a round bottom glass flask, aldehyde (1.7 mmol), malononitrile (1.7 mmol), DCM (3 mL), and catalyst (100 mg) were charged. The reaction mixture was stirred at ambient temperature

for the desired time period. A Teflon lined closed autoclave was used when the reaction was performed at higher temperatures. After completion of the reaction, the catalyst was removed by centrifugation and the reaction mixture was analyzed by gas chromatography (GC) (Yonglin; 6100; BP-5; 30 m×0.25 mm×0.25 μm). The identification of the products was carried out with Gas chromatograph-Mass spectrometer (GC-MS) (Shimadzu GCMS-QP 2020 NX) and ^{1}H NMR spectroscopy. The formation and purities of condensation products of FAL, HMF, and DFF are confirmed from ^{1}H and ^{13}C NMR spectroscopy.

^{1}H &^{13}C NMR data of various Biginelli products synthesized in this study.

(a) NMR data of FAL derived product (I) (5-acetyl-4-(furan-2-yl)-6-methyl-3,4-dihydropyrimidin-2(1H)-one)

^{1}H NMR (400 MHz, DMSO-d_6): δ 9.21 (d, 1H), 7.84 (dd, 1H), 7.52 (d, 1H), 6.32 (dd, 1H), 6.07 (d, 1H), 5.26 (d, 1H), 2.20 (s, 3H), 2.12 (s, 3H).

^{13}C NMR (400 MHz, DMSO-d_6): δ 194.3, 156.4, 153.0, 149.4, 142.9, 110.8, 107.8, 106.1, 48.4, 30.5, 19.5.

(b) NMR data of HMF derived product (II) (5-acetyl-4-(5-(hydroxymethyl)furan-2-yl)-6-methyl-3,4-dihydropyrimidin-2(1H)-one)

^{1}H NMR (400 MHz, DMSO-d_6): δ 9.23 (d, 1H), 7.87 (dd, 1H), 6.15 (d, 1H), 6.02 (d, 1H), 5.27 (d, 1H) 5.18 (t, 1H), 4.33 (d, 2H), 2.25 (s, 3H), 2.17 (s, 3H).

^{13}C NMR (400 MHz, DMSO-d_6): δ 193.9, 155.2, 154.9, 152.4, 149.0, 107.7, 107.1, 106.3, 55.7, 47.8, 30.1, 19.0.

(c) NMR data of DFF derived product (III) (4,4'-(furan-2,5-diyl)bis(5-acetyl-6-methyl-3,4-dihydropyrimidin-2(1H)-one))

^{1}H NMR (400 MHz, DMSO-d_6): δ9.21 (d, 2H), 7.83 (dd, 2H), 6.22 (d, 2H), 5.26 (d, 2H), 2.20 (s, 6H), 2.12 (s, 6H).

^{13}C NMR (400 MHz, DMSO-d_6): δ 194.2, 154.2, 152.3, 149.6, 107.1, 106.3, 47.8, 30.2, 19.3.

(d) NMR data of Benzaldehyde derived product (IV) (5-acetyl-6-methyl-4-phenyl-3,4-dihydropyrimidin-2(1H)-one)

^{1}H NMR (400 MHz, DMSO-d_6): δ 9.19 (d, 1H), 7.83 (dd, 1H), 7.21-7.36 (m, 5H), 5.25 (d, 1H), 2.28 (s, 3H), 2.10 (s, 3H).

^{13}C NMR (400 MHz, DMSO-d_6): δ 194.8, 152.5, 148.9, 144.7, 129.1, 127.7, 126.9, 109.9, 54.5, 30.8, 19.4.

^{1}H &^{13}C spectroscopic data of various Knoevenagel condensation products synthesized in this study.

(a) NMR data of FAL derived product: (2-(furan-2-ylmethylene)malononitrile)

^{1}H NMR (400 MHz, DMSO-d_6): δ 7.81 (d, 1H), 7.52 (s, 1H), 7.35 (d, 1H), 6.71 (m, 1H).

^{13}C NMR (400 MHz, DMSO-d_6): δ149.8, 148.0, 143.2, 123.7, 114.6, 114.0, 112.7, 77.4.

(b) NMR data of HMF derived product: (2((5-hydroxymethylfuran-2-yl)methylene)malononitrile)

^{1}H NMR (400 MHz, DMSO-d_6): δ 8.19 (s, 1H), 7.42 (d, 1H), 6.73 (d, 1H), 4.52 (s, 1H), 3.52 (s, 1H).

^{13}C NMR (400 MHz, DMSO-d_6): δ 164.7, 147.4, 144.2, 127.2, 114.9, 113.6, 111.9, 73.9, 56.2.

(c) NMR data of DFF derived product: (2,2`-(furan-2,5-diylbis(methanylylidene))dimalononitrile)

^{1}H NMR (400 MHz, DMSO-d_6): δ8.47 (s, 1H), 7.67 (s, 1H).

^{13}C NMR (400 MHz, DMSO-d_6): δ149.8, 143.1, 123.8, 114.5, 114.0, 77.1.

Physicochemical Characterization

$ZrPO_4$, $TiPO_4$, and $SnPO_4$ exhibit a broad XRD pattern with a peak maximum at $2\theta = 27°$ suggesting that the materials are amorphous in nature (Figure S1). Such amorphous nature is well-established for the $TiPO_4$ synthesized using block copolymers as mesopore directing agent.[R1] The N_2-sorption analysis is carried out to analyze the textural properties of all the metal phosphates (Figure S2a,b). $ZrPO_4$ shows a type IV isotherm with H3 hysteresis loop. H3 hysteresis does not exhibit any limiting adsorption at high P/P_0 and suggests the presence of non-rigid aggregates of plate-like particles or having slit-shape pores. $TiPO_4$ exhibits a type IV isotherm with H1 hysteresis loop. $TiPO_4$ exhibits a steep increase in the N_2 adsorption above 0.45 and extends up to 0.9 (P/P_0) confirming the presence of well-defined mesopores in the material. BJH pore size distribution shows that $ZrPO_4$ exhibits a non-uniform pore size distribution in the range of 2-10 nm with a peak maximum of 2.5 nm whereas $TiPO_4$ exhibits a well-defined pore size distribution in the range of 3-8 nm with peak maximum of 5.5 nm. The signature of isotherms is consistent with the BJH pore size distribution observed in $ZrPO_4$ and $TiPO_4$. $SnPO_4$ exhibits type IV isotherm with the H4 hysteresis loop. $SnPO_4$ exhibits very low adsorption volume in the pressure range of 0-0.6 (P/P_0). A steep increase in the N_2 adsorption above 0.6 (P/P_0) suggests that material has broad interconnected meso-macropores. BJH pore size distribution shows that $SnPO_4$ exhibits a very low-intensity broad pore size distribution when compared to the other two materials. The textural properties of various metal phosphates synthesized in this study are summarized in Table S1. The largest surface area and external surface area are obtained for $ZrPO_4$ whereas the largest pore volume is obtained for $TiPO_4$. $SnPO_4$ exhibits the lowest surface area and pore volume among the materials prepared in this study. For comparative purposes, crystalline $ZrPO_4$ was also prepared. XRD pattern shows that the material is highly crystalline and matches well with α-$ZrPO_4$ phase reported in the literature (Figure S3a).[R3] N_2-sorption analysis suggests that the material exhibits very low N_2 adsorption with a wide pore size distribution in the range of 10-200 nm with a peak maximum of 102 nm (Figure S3b). The surface area and pore volume of crystalline $ZrPO_4$ are determined to be 9.8 m^2/g and 0.102 mL/g, respectively.

The microstructural and morphological details of the synthesized catalysts were examined using a scanning electron microscope. All the metal phosphates prepared in this study exhibit aggregated morphology. $TiPO_4$ and $SnPO_4$ exhibit dispersed non-uniform submicrometer to micrometer size crystal morphology whereas $ZrPO_4$ exhibits aggregated

non-uniform morphology (Figure S4a-d). Crystalline $ZrPO_4$ exhibits aggregated crystals forming layered like morphology (Figure S4e). The magnified image of $ZrPO_4$ shows that the large microcrystals are built with small 100-200 nm nanocrystals. The nanoscale morphology and elemental distribution were investigated for highly active $ZrPO_4$ using transmission electron microscopy (TEM). Figures S2c & d, confirms the aggregated morphology of $ZrPO_4$ which is consistent with the SEM morphology discussed above. The high-resolution TEM image (HR-TEM) confirms that 50-100 nm size crystals built the aggregated morphology. Moreover, no distinguishable lattice fringes are observed in the HR-TEM image confirming the amorphous nature of the material (Figure S2d). Further, the electron diffraction pattern (Figure S2d, inset) also suggests the amorphous nature of the material, which is consistent with the XRD measurement. Figure S5a-d presents the elemental mapping of Zr, P, and O elements obtained from TEM image. It shows the uniform distribution of these elements throughout the material. Figure S5e presents the energy dispersive x-ray analysis (EDX) of $ZrPO_4$ that further confirms the presence of Zr, P, and O elements in the material.

The X-ray photoelectron spectroscopic analysis was carried out for the investigation of surface chemical composition and oxidation states of various elements present in $ZrPO_4$. Figure S6a presents the complete surface survey of the $ZrPO_4$ catalyst confirming the presence of Zr, P, and O elements in $ZrPO_4$. To examine the oxidation states of various elements present in $ZrPO_4$, the high-resolution spectra were recorded, individually, for these elements. In the high-resolution spectrum of Zr 3d, two peaks with binding energies 184.1 eV and 186.2 eV can be assigned to $3d_{5/2}$ and $3d_{3/2}$ electronic configurations, respectively, for Zr present in $ZrPO_4$ (Figure S6b).[R5] The high-resolution spectrum of P 2p exhibits one broad intense peak which corresponds to the phosphorous in P^{+5} oxidation state that can be deconvoluted to $2p_{1/2}$ and $2p_{3/2}$ (Figure S6c).[R5] Similar to phosphorous, the high-resolution surface survey of O 1s presents only a single broad peak that can be deconvoluted into two peaks centered at 531.6 eV and 533.5 eV (Figure S6d). The peak with binding energy 531.6 eV corresponds to the oxygen present as Zr—O—P (can be co-existed with P=O and Zr-O-X (where X = P or H) while the peak at 533.5 eV is attributed to a hydroxyl group (P—O—H) present in $ZrPO_4$.[R5] These results confirm the presence of Zr, P, and O elements in their proper oxidation states and suggest the successful formation of $ZrPO_4$. The presence of Zr—O—P and P—O—H suggests that the material has basic bridging “O” sites and acidic sites (Lewis acidic sites due to Zr sites and Brönsted acidic sites due to P-O-H groups).

The recyclability of the catalyst in FAL to FOL conversion

$ZrPO_4$ was recycled for five times during the FAL conversion to FOL in isopropanol. After the reaction, the catalyst was recovered, washed with isopropanol followed by ethanol and then dried at 473 K for 4 h and then used in the next cycle. Catalytic activity data suggest that no significant decrease in the activity is observed (Figure S11a). XRD and SEM investigation reveals that no change in the XRD or morphology is observed after five recycles (Figure S12). A hot-filtration test was carried out to confirm the heterogeneity of the catalytic process. The catalyst was removed after 4 h of the reaction and the reaction was conducted without the catalyst for the remaining 8 h. The analysis shows that no significant increase in FAL conversion is observed after the removal of the catalyst from the reaction mixture suggesting that the reaction takes place on the catalyst surface (Figure S11b). Moreover, leaching of the catalyst did not take place which catalyzes further reaction. Further, the stability test was carried out in 2-propanol and water at 120 °C (Figure S13). Catalysts were subjected to XRD measurement after 6 h and 24 h. XRD measurements confirm that the catalysts recovered from 2-propanol after 6 h and 24 h exhibit similar XRD pattern to that of the fresh catalyst (Figure S13a). Moreover, the solution was very transparent in nature and no leaching of Zr was detected by ICP analysis (Figure S13c). XRD measurement confirms that the catalysts recovered from the water after 6 h and 24 h show the appearance of a peak at 18 ° confirming the occurrence of phase change upon heating in water (Figure S13b). Moreover, the solution was found to be turbid and leaching of Zr was detected by ICP analysis (Figure S13c). The amount of sample loss was 14 wt% after 24 h of heat treatment in water. Thus it is confirmed that the present catalyst can be efficiently recyclable in the 2-propanol medium.

The details of FAL adsorption using Zeta Potential measurement

The influence of adsorption is also investigated through zeta potential measurement. In each step, the consistency of the data is monitored by repeating the analysis for three times. Zeta potential is measured to be -1.8 mV for 10 mL of isopropanol. Upon the addition of 100 mg of $ZrPO_4$, the zeta potential is increased to -0.1 mV. It is reported in the literature that with an increase in the hydrophilicity, the zeta potential increases.[R6] $ZrPO_4$ has large numbers of surface -OH groups that increase the hydrophilicity. Upon addition of 1 mmol of FAL to the above reaction mixture, the zeta potential is reduced to -0.4 mV which suggests that FAL adsorption on the catalyst surface decreases the hydrophilicity by the adsorption through furan carbonyl and thus the zeta potential is reduced.

The details of HMF/DFF reduction

HMF reduction is carried out at a different temperature in the range of 353 K – 403 K for the different time periods. Reaction conducted at 353 K shows that the desired product is not obtained even up to17 h. At the beginning of the reaction, 5-methylfurfuryl alcohol is obtained in large selectivity. With an increase in reaction time, 5-methyl furfural alcohol selectivity decreases and 2-(isopropoxymethyl)-5-methylfuran selectivity increases which suggests that methyl substitution favors the etherification reaction. The small concentration of 5-methyl furfural suggests that the reduction of $–CH_2OH$ group in HMF is preferred over –CHO group. This is the reason, desired product 2,5-bis(hydroxymethyl)furan is not obtained at all under this condition. When the same reaction is performed at 383 K, very low selectivity of the desired product 2,5-bis(hydroxymethyl)furan is obtained. In this case, four products are obtained as shown in Table S4. The best selectivity of the desired product is obtained after 0.5 h of the reaction carried out at 393 K. With increase in the time, the selectivity of the desired product decreases and the selectivity of 2-(isopropoxymethyl)-5-methylfuran increases and 2-(isopropoxymethyl)-5-methylfuran is obtained as the major product at the end of the reaction. Interestingly, when the same reaction is performed at a higher temperature of 403 K then the desired product selectivity 2,5-bis(hydroxymethyl)furan did not improve but instead, the 2-(isopropoxymethyl)-5-methylfuran is observed in very high yield just in 3 h. Thus, temperature-dependent and the time-dependent catalytic investigation clearly suggest the pathway for the reduction of HMF (Scheme S1). The higher yield of 2,5-bis(hydroxymethyl)furan in the case of DFF is observed because both the aldehyde groups has to be reduced first and then the one $–CH_2OH$ group gets reduced and the second one reacts with propanol to form 2-(isopropoxymethyl)-5-methylfuran as the large product at the end of 6 h of the reaction (Table 1, entry 8).

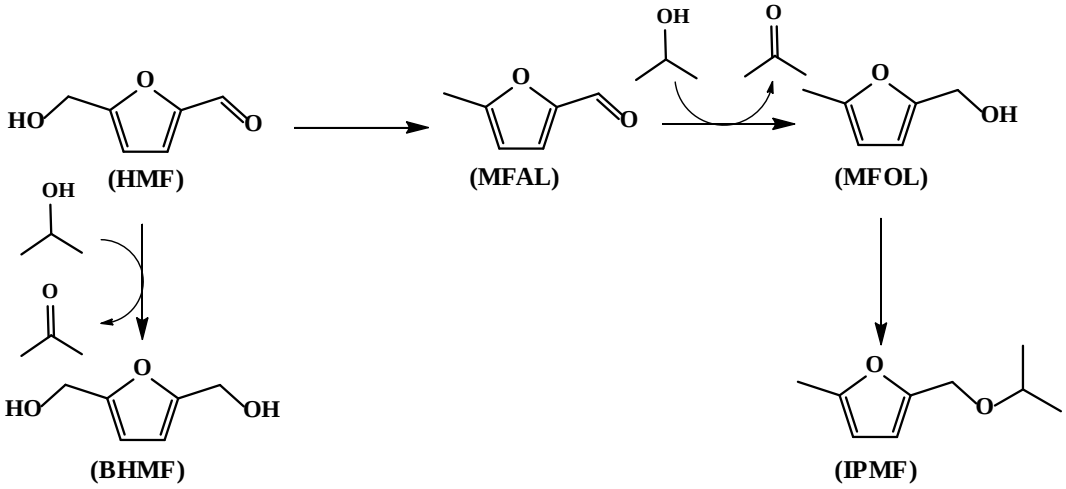

Scheme S1. Suggested pathway for HMF reduction using isopropanol over $ZrPO_4$ catalyst.

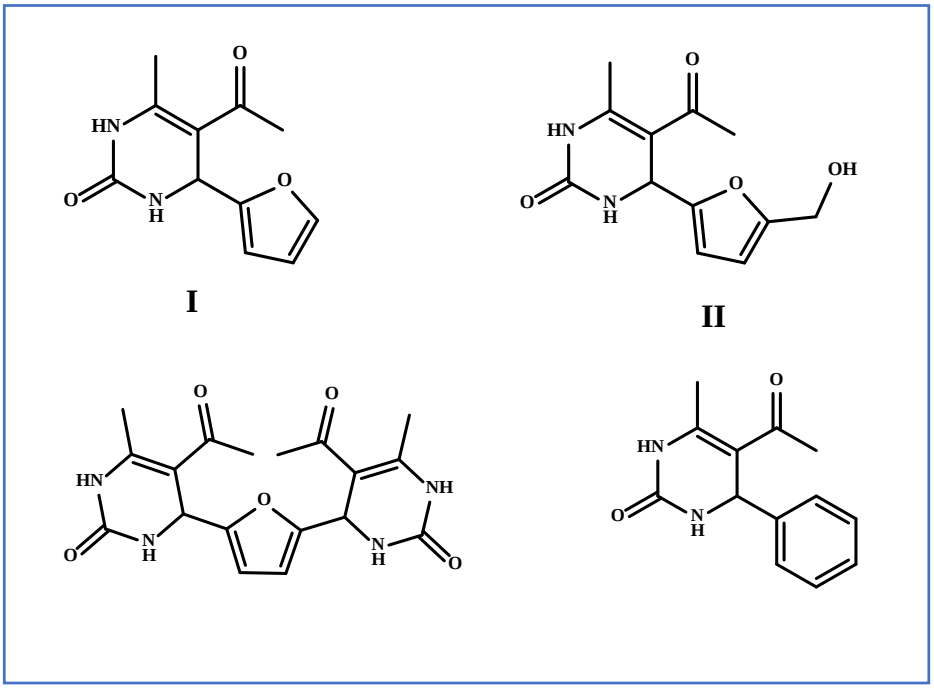

Scheme S2. Various Biginelli products synthesized in this study.

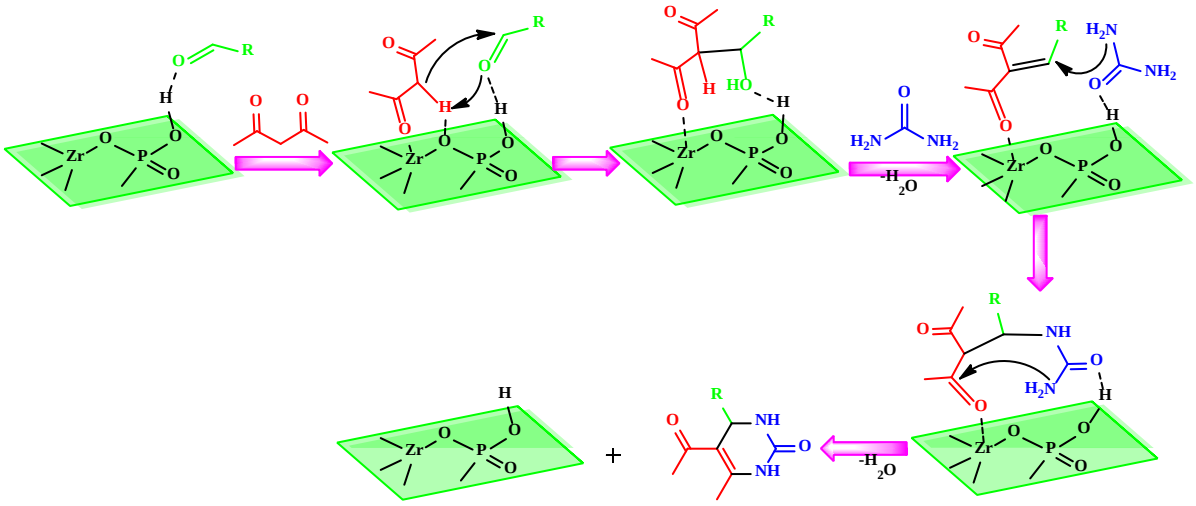

Scheme S3. The plausible reaction mechanism for the synthesis of Biginelli product over $ZrPO_4$ catalyst.

Control reactions and Description of the Mechanism: The Zr and P—OH sites present in the catalyst acting as the Lewis and Brönsted acid sites, respectively. In order to propose the reaction mechanism, three control reactions are performed. FAL is reacted with acetylacetone, the FAL is reacted with urea, and acetylacetone is reacted with urea in the presence of $ZrPO_4$. No product is observed after 4 h of the reaction for the reaction mixture containing FAL and urea measured using ^{1}H NMR. Similarly, no product is observed after 4 h of the reaction for the reaction mixture containing acetylacetone and urea measured using ^{1}H NMR. However, a product is observed after 4 h of the reaction for the reaction mixture containing FAL and acetylacetone measured using ^{1}H NMR. The control reactions suggest that first FAL and acetylacetone are reacted to form the intermediate, which further reacts with urea to form the desired Biginelli product.

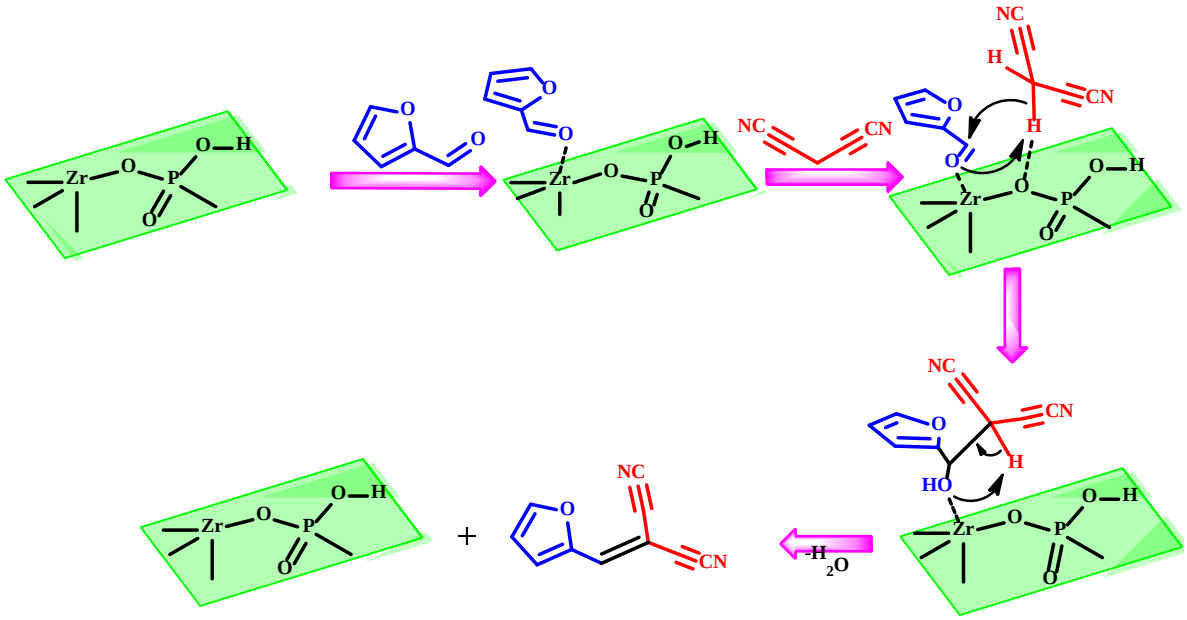

Scheme S4. The plausible reaction mechanism for Knoevenagel condensation reaction over $ZrPO_4$ catalyst.

Description of the Mechanism: In the first step, a FAL molecule adsorbs on the catalyst surface through the interaction between C=C and C=O bonds of FAL. Malononitrile adsorption takes place on the basic sites of $ZrPO_4$ through activated acidic –C-H of malononitrile. In the next step, the carbonyl oxygen of FAL abstracts the activated –C-H proton and forms an alcohol intermediate which upon dehydration produces the desired product.

Table S1. Textural properties of various metal phosphates synthesized in this study.

E. no.	Catalyst	S_{BET} (m^2g^{-1})	S_{Ext} (m^2g^{-1})	V_{total} (cc g^{-1})	D_{avg} (nm)	$T_{acidity}$ (mmol/g)	$T_{basicity}$ (mmol/g)
1	$ZrPO_4$	232	187	0.280	4.3	0.17	0.12
2	$TiPO_4$	193	157	0.324	10.3	0.22	0.18
3	$SnPO_4$	52	48	0.165	3.8	0.06	0.06

S_{BET} was calculated from the adsorption branch in the relative pressure range of $0.05 < P/P_0 \leq 0.3$. S_{BET} = total surface area, S_{Ext} = external surface area, V_{total} = total pore volume, D_{avg} = average pore diameter, $T_{acidity}$ = total acidity, and $T_{basicity}$ = total basicity.

Table S2. Transfer hydrogenation of FAL over $ZrPO_4$ using various alcohols as a hydrogen donor.

E. no.	Catalyst	Substrate	Solvent	Conv. (%)	Selectivity (%)
1.	$ZrPO_4$	Furfural	2-propanol	95.2	FOL (76), IPMF (24)
2.	$ZrPO_4$	Furfural	Methanol	51.1	FOL (5), MMF (11), DMMF (85)
3.	$ZrPO_4$	Furfural	Ethanol	60.3	FOL (11), EMF (17), DEMF (68)
4.	$ZrPO_4$	Furfural	n-propanol	75.1	FOL (16), PMF (22), DPMF (62)
5.	$ZrPO_4$	Furfural	n-butanol	83.4	FOL (22), BMF (25), DBMF (53)

Reaction condition: FAL (1mmol), catalyst (50 mg), solvent (7 ml), temperature (393 K), reaction time (6 h).

Furfuryl alcohol (FOL), 2-(isopropoxymethyl)furan (IPMF), methoxymethylfuran (MMF), 2-(dimethoxymethyl)furan (DMMF), ethoxymethylfuran (EMF), 2-(diethoxymethyl)furan (DEMF), propoxymethylfuran (PMF), butoxymethylfuran (BMF), 2-(dipropoxymethyl)furan (DPMF), 2-(dibutoxymethyl)furan (DBMF).

Table S3. Comparative catalytic activity data in the transfer hydrogenation of furfural to furfural alcohol over reported catalysts with $ZrPO_4$.

E. no.	Catalysts	FAL conv. (%)	FOL selec. (%)	FOL Yield (%)	Reaction condition	Ref. no.
1	γ-Fe_2O_3@HAP	96.2	95.3	91.7	Furfural (1 mmol), 2-propanol (15 mL), catalyst (40 mg), 10 h, 453 K, 10 bar N_2	R7
2	Al–Zr@Fe_3O_4	99.1	-	90.5	Furfural (2 mmol), 2-propanol (10 mL), catalyst (40 mg), 4 h, 453 K	R8
3	N-doped carbon supported Fe	91.6	83.0	-	Furfural (0.5 mmol), 2-butanol (3 mL), catalyst (50 mg), 15 h, 433 K	R9
4	Cu/MgO-Al_2O_3	100	-	89.3	Furfural (1.04 mmol), 2-propanol (5 mL), catalyst (50 mg), 1 h, 483 K	R10
5	Zr-Hydroxyphosphonoacetate	98	-	96	Furfural (1 mmol), 2-propanol (5 mL), catalyst (75 mg), 1.5 h, 423 K	R11
6	Fe_3O_4@C	93.6	98.9	-	Furfural (2 mmol), 2-propanol (10 mL), catalyst (50 mg), 4 h, 473 K, 20 bar N_2	R12
7	Zr-phosphotungstate	98.7	98.9	98.6	Furfural (1 mmol), 2-propanol (5 mL), catalyst (200 mg), 1 h, 393 K	R13
8	ZrO_2	48.2	98.1	-	Furfural (1 mL), 2-propanol (9 mL), catalyst (50 mg), 24 h, 373 K	R14
9	$Zr(OH)_2$	100	-	98.9	Furfural (1.2 mmol), 2-propanol (15 mL), catalyst (75 mg), 2.5 h, 443 K, 10 bar N_2	R15
10	Cu-Mg-Al	100	100	100	Furfural (0.2 M), 2-propanol (60 mL), catalyst (200 mg), 8 h, 423 K, inert atm. (N_2)	R16
11	γ-Al_2O_3	100	-	>90	2-propanol/Furfural molar ratio (50),	R17

					furfural/catalyst mass ratio (1), 6 h, 423 K	
12	NiO	98.9	-	94.4	Furfural (2 mmol), 2-propanol (10 mL), catalyst (80 mg), 0.5 h, 443 K	R18
13	$ZrPO_4$	95.1	76.0	-	Furfural (1 mmol), 2-propanol (7 mL), catalyst (50 mg), 6 h, 393 K, inert atm. (N_2)	This study

Table S4. Influence of reaction temperature on the catalytic activity of $ZrPO_4$ in the transfer hydrogenation reaction of HMF in 2-propanol.

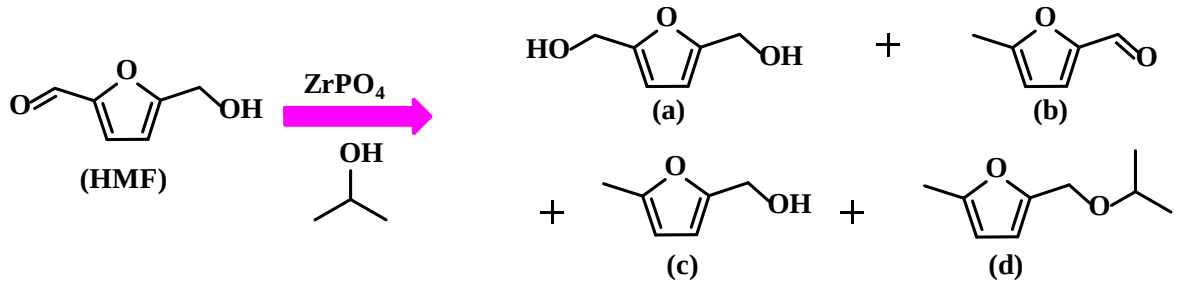

E. no.	Substrate	Substrate Conversion (%)	Product selectivity (%)				Temp. (K)	Time (h)
			A	B	c	d		
1.	HMF	10.3	0	0.5	72.3	27.2	353	1
		20.2	0	1.5	58.1	40.4		3
		31.5	0	2.5	48.7	48.8		5
		38.6	0	3.0	32.8	64.2		8
		44.1	0	3.9	23.2	72.9		11
		49.0	0	4.6	16.6	78.8		14
		52.5	0	6.6	9.2	84.2		17
2.	HMF	54.2	4.8	4.3	46.9	44.0	383	1
		72.4	2.5	4.1	33.4	60.0		3
		93.3	2.0	3.8	23.7	70.5		6
3.	HMF	44.5	32.0	2.8	50.4	14.8	393	0.5
		63.1	25.0	1.8	42.2	31		1
		88.2	18	2.2	29.8	50		3
		100	9.6	3.4	10	77		6
4.	HMF	75	0.8	5.2	38.4	55.6	403	1
		98	0	3.9	14.6	81.5		3

Reaction condition: HMF (1mmol), catalyst $ZrPO_4$ (50 mg), and 2-propanol (7 ml).

Table S5. The eco-score calculation for FAL to FOL conversion over $ZrPO_4$.

Details of parameters	Penalty points
1. Yield (72.2 %)	13.9
2. Price of reaction components (to obtain 10 mmol of products)	
Inexpensive (< $10)	0
Expensive (> $10 and < $50)	0
Very expensive (> $50)	0
3. Safety[a]	
N (dangerous for the environment)	0
T (toxic)	0
F (highly flammable)	5
E (explosive)	0
F^+(Extremely flammable)	0
T^+(Extremely toxic)	0
4. Technical setup	0
Common setup	0
Instruments for controlled addition of chemicals[b]	0
Unconventional activation technique[c]	0
Pressure equipment, > 1 atm[d]	0
Any additional special glassware 1	0
(Inert) gas atmosphere	1
Glovebox	0
5. Temperature/time	
Room temperature, < 1 h	0
Room temperature, < 24 h	0
Heating, < 1 h	0
Heating, > 1 h	3
Cooling to 0°C	0
Cooling, < 0°C	0
6. Workup and purification	
Cooling to room temperature	0
Adding solvent	0
Simple filtration	0
Removal of solvent with bp<150^0C	0
Crystallization and filtration	0
Removal of solvent with bp> 150°C	0
Solid-phase extraction	0
Distillation	0
Sublimation	0
Liquid-liquid extraction[e]	0
Classical chromatography	0

Eco-Score = 100-23.9 = **76.1**

E-factor calculation for the FAL to FOL conversion over $ZrPO_4$

Total amount of reactants: 0.096 g, Amount of final product: 0.071 g, E-Factor = amount of waste/amount of product = 0.031/0.071= **0.43**

Table S6. The eco-score calculation for FAL derived Biginelli product formation over $ZrPO_4$.

Details of parameters	Penalty points
1. Yield (94.0 %)	3
2. Price of reaction components (to obtain 10 mmol of products)	
Inexpensive (< $10)	0
Expensive (> $10 and < $50)	0
Very expensive (> $50)	0
3. Safety	
N (dangerous for environment)	5 (acetyl acetone)
T (toxic)	0
F (highly flammable)	0
E (explosive)	0
F^+(Extremely flammable)	0
T^+(Extremely toxic)	0
4. Technical setup	0
Common setup	0
Instruments for controlled addition of chemicals[b]	0
Unconventional activation technique[c]	0
Pressure equipment, > 1 atm[d]	0
Any additional special glassware 1	0
(Inert) gas atmosphere	0
Glovebox	0
5. Temperature/time	
Room temperature, < 1 h	0
Room temperature, < 24 h	1
Heating, < 1 h	0
Heating, > 1 h	0
Cooling to 0°C	0
Cooling, < 0°C	0
6. Workup and purification	
Cooling to room temperature	0
Adding solvent	0
Simple filtration	0
Removal of solvent with bp<150^0C	0
Crystallization and filtration	0
Removal of solvent with bp> 150°C	0
Solid-phase extraction	0
Distillation	0
Sublimation	0
Liquid-liquid extraction[e]	0
Classical chromatography	0

Eco-Score = 100-9 = **91**

E-factor calculation for FAL derived Biginelli product formation over $ZrPO_4$

Total amount of reactants: 0.392 g, Amount of final product: 0.2068 g, E-Factor = amount of waste/amount of product = 0/0.2068 = **0.0**

Table S7. The eco-score calculation for FAL conversion in Knoevenagel condensation reaction over $ZrPO_4$.

Details of parameters	Penalty points
1. Yield (99 %)	0.5
2. Price of reaction components (to obtain 10 mmol of products)	
Inexpensive (< $10)	0
Expensive (> $10 and < $50)	0
Very expensive (> $50)	0
3. Safety[a]	
N (dangerous for the environment)	5 (malononitrile)
T (toxic)	5 (malononitrile)
F (highly flammable)	0
E (explosive)	0
F^+(Extremely flammable)	0
T^+(Extremely toxic)	0
4. Technical setup	0
Common setup	0
Instruments for controlled addition of chemicals[b]	0
Unconventional activation technique[c]	0
Pressure equipment, > 1 atm[d]	0
Any additional special glassware 1	0
(Inert) gas atmosphere	0
Glovebox	0
5. Temperature/time	
Room temperature, < 1 h	0
Room temperature, < 24 h	1
Heating, < 1 h	0
Heating, > 1 h	0
Cooling to 0°C	0
Cooling, < 0°C	0
6. Workup and purification	
Cooling to room temperature	0
Adding solvent	0
Simple filtration	0
Removal of solvent with bp<150^0C	0
Crystallization and filtration	0
Removal of solvent with bp> 150°C	0
Solid-phase extraction	0
Distillation	0
Sublimation	0
Liquid-liquid extraction[e]	0
Classical chromatography	0

Eco-Score = 100-11.5 = **88.5**

E-factor calculation for FAL conversion in Knoevenagel condensation reaction over $ZrPO_4$.

Total amount of reactants: 0.275 g, Amount of final product: 0.142 g, E-Factor = amount of waste/amount of product = 0/0.142= **0.0**

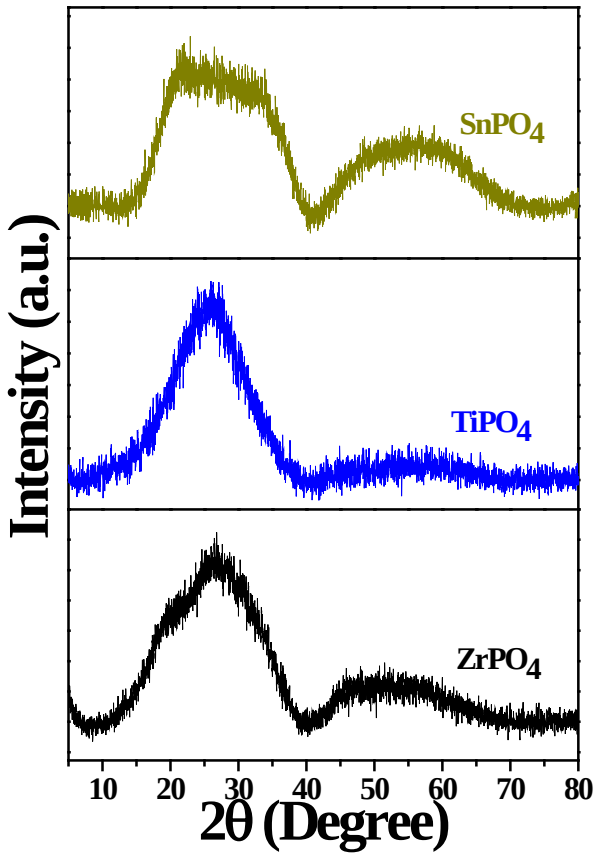

Figure S1. Powder XRD-patterns of synthesized metal phosphates.

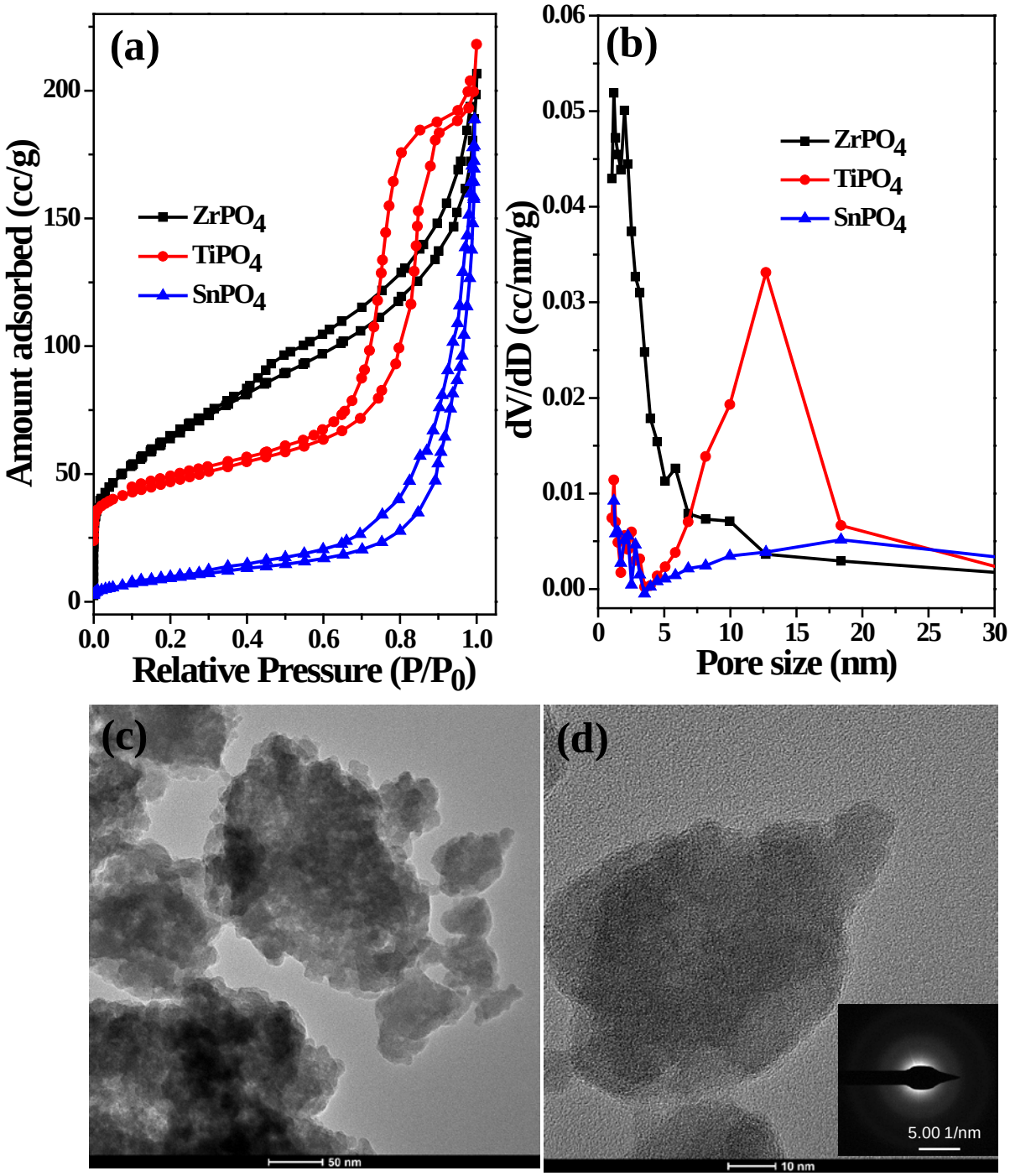

Figure S2. (a) N_2-sorption isotherms and (b) BJH pore size distribution for the metal phosphates synthesized in this study, (c, d) TEM images of $ZrPO_4$ (inset in Figure d presents the electron diffraction pattern).

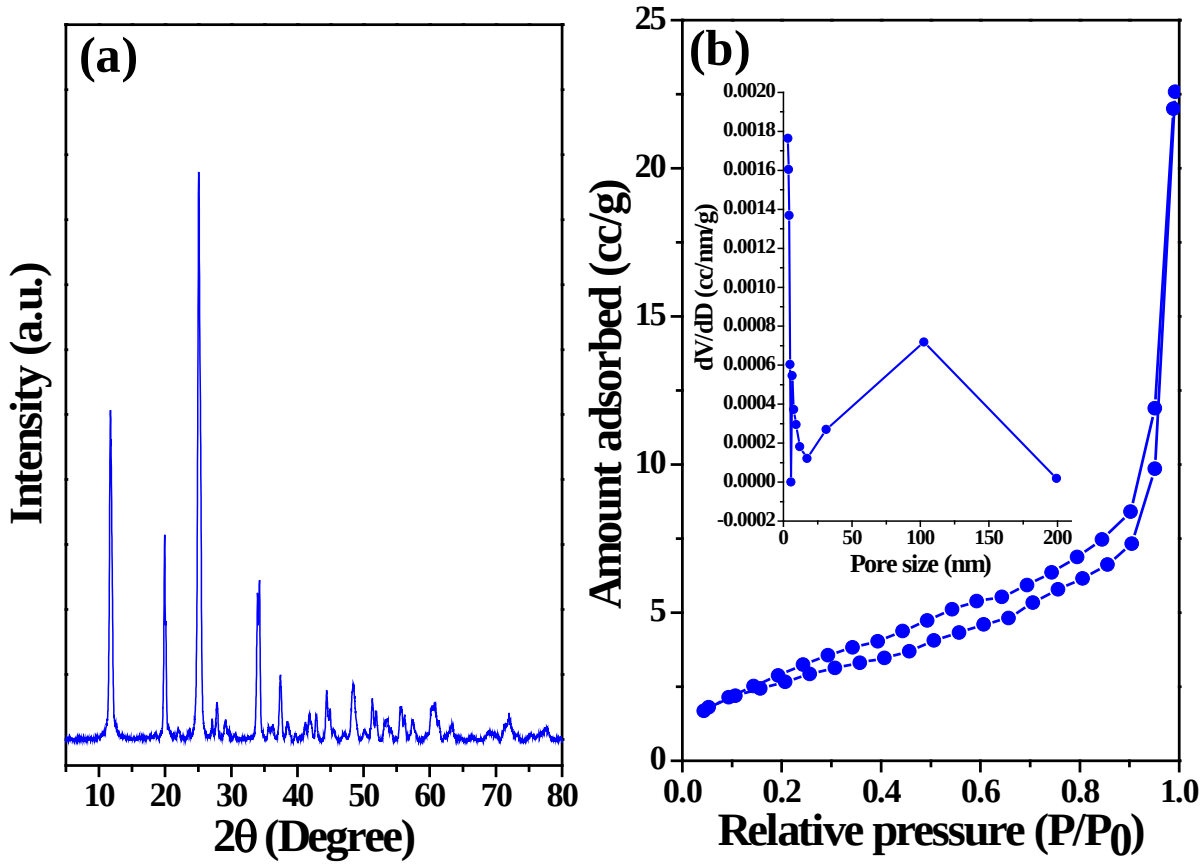

Figure S3. (a) Powder XRD-pattern and (b) N_2-sorption isotherm of crystalline $ZrPO_4$. Inset of (b) shows the BJH pore size distribution.

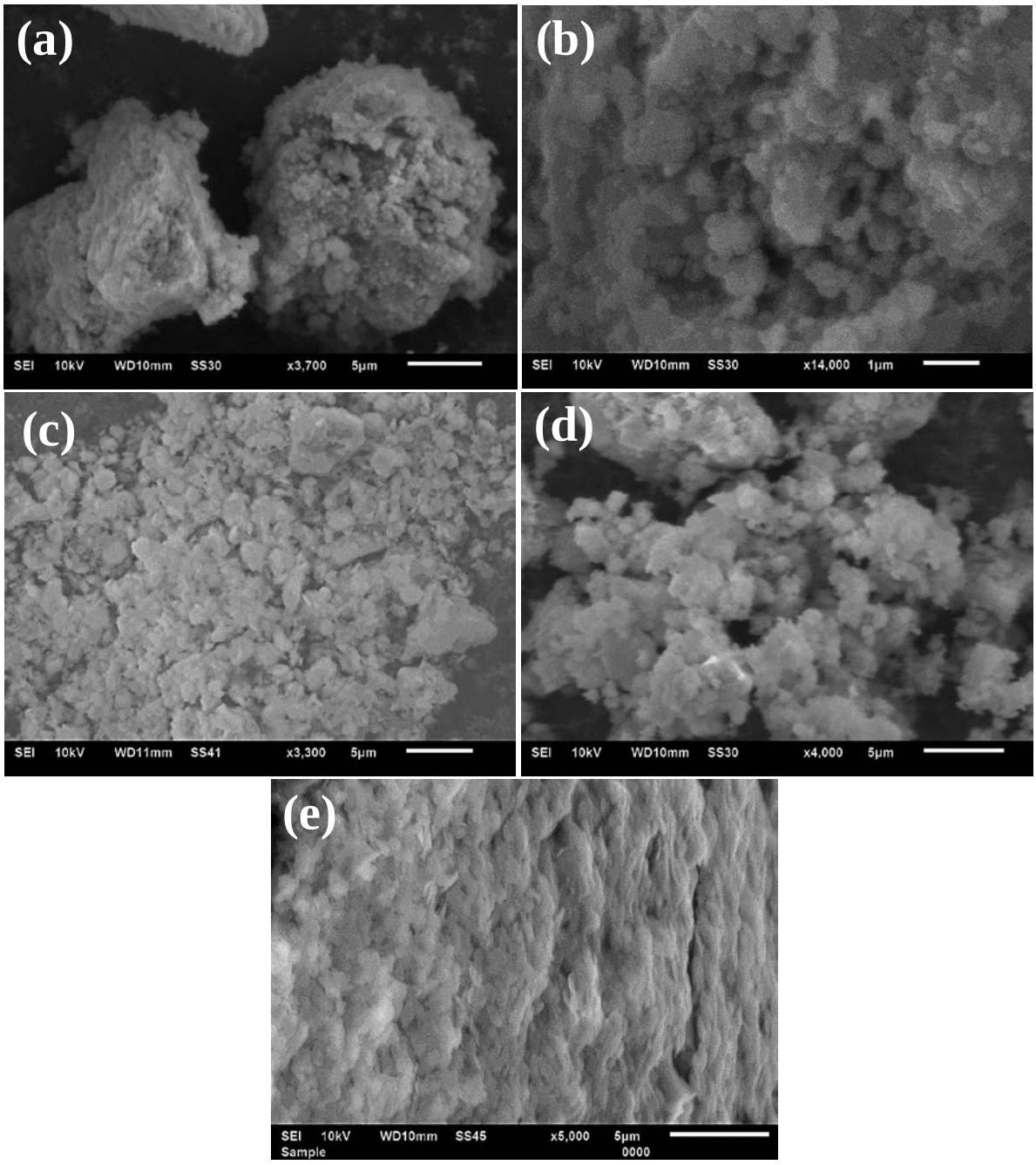

Figure S4. SEM images of (a, b) $ZrPO_4$ catalyst, (c) $SnPO_4$, (d) $TiPO_4$, and (e) crystalline $ZrPO_4$.

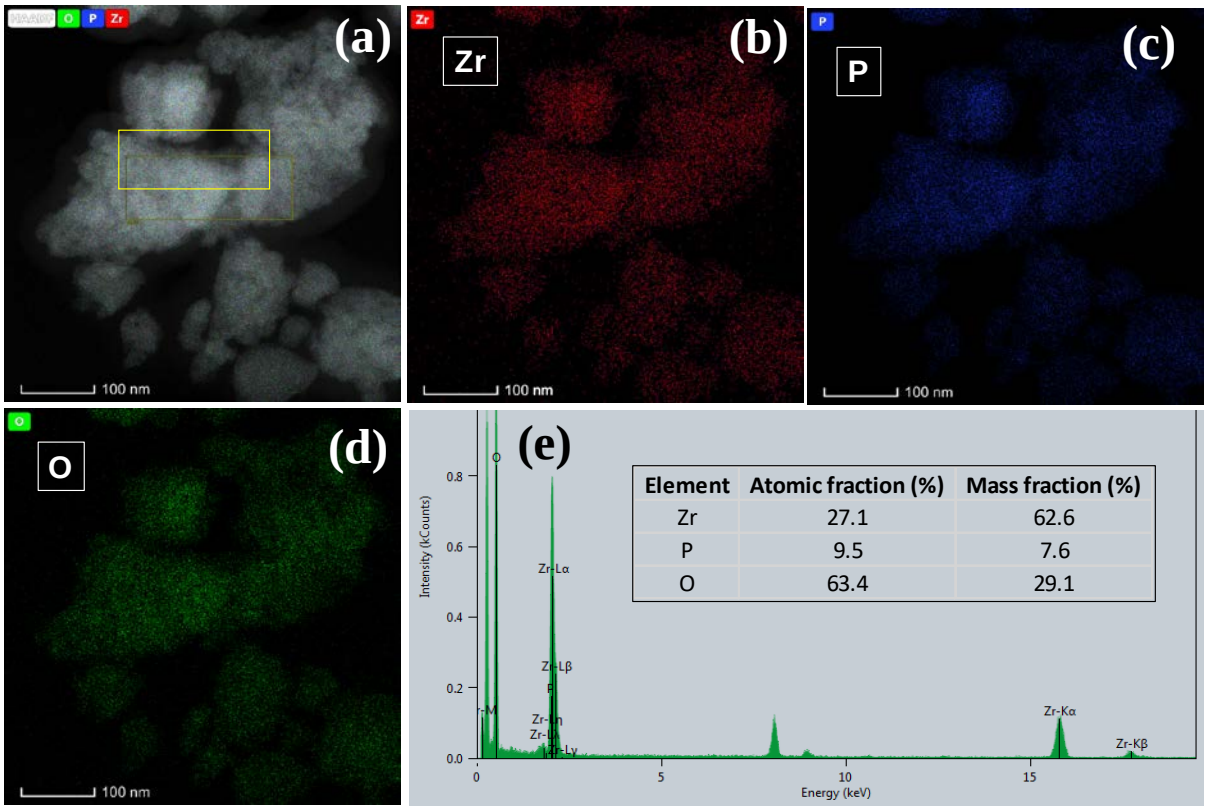

Figure S5. (a) TEM image selected for elemental mapping, (b) elemental mapping for Zr, (c) elemental mapping for P, (d) elemental mapping for O, and (e) EDS spectrum of $ZrPO_4$ recorded from the yellow domain selected in Figure a.

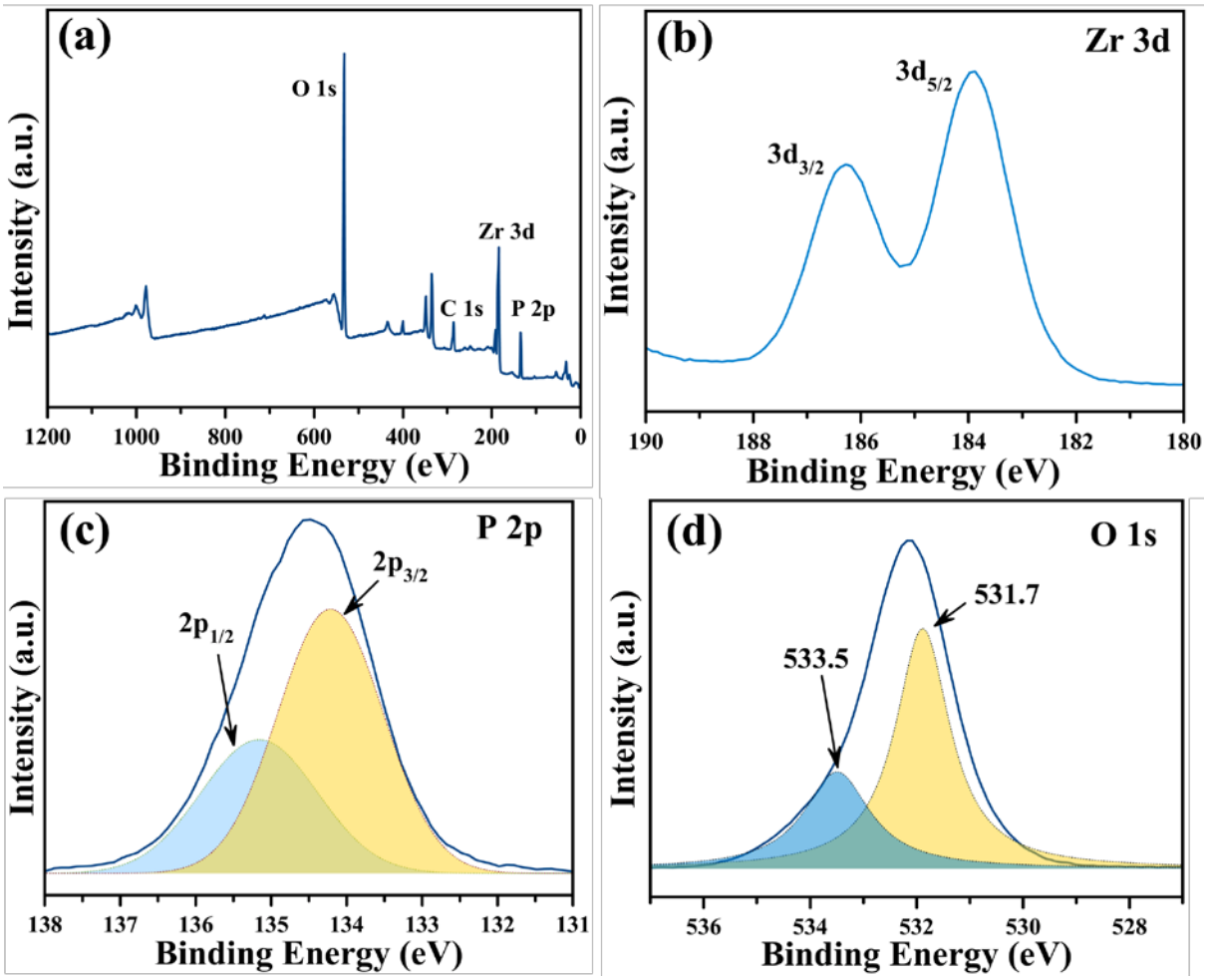

Figure S6. (a) XPS surface survey of $ZrPO_4$, high-resolution XPS spectra of (b) Zr 3d, (c) P 2p, and (d) O 1s.

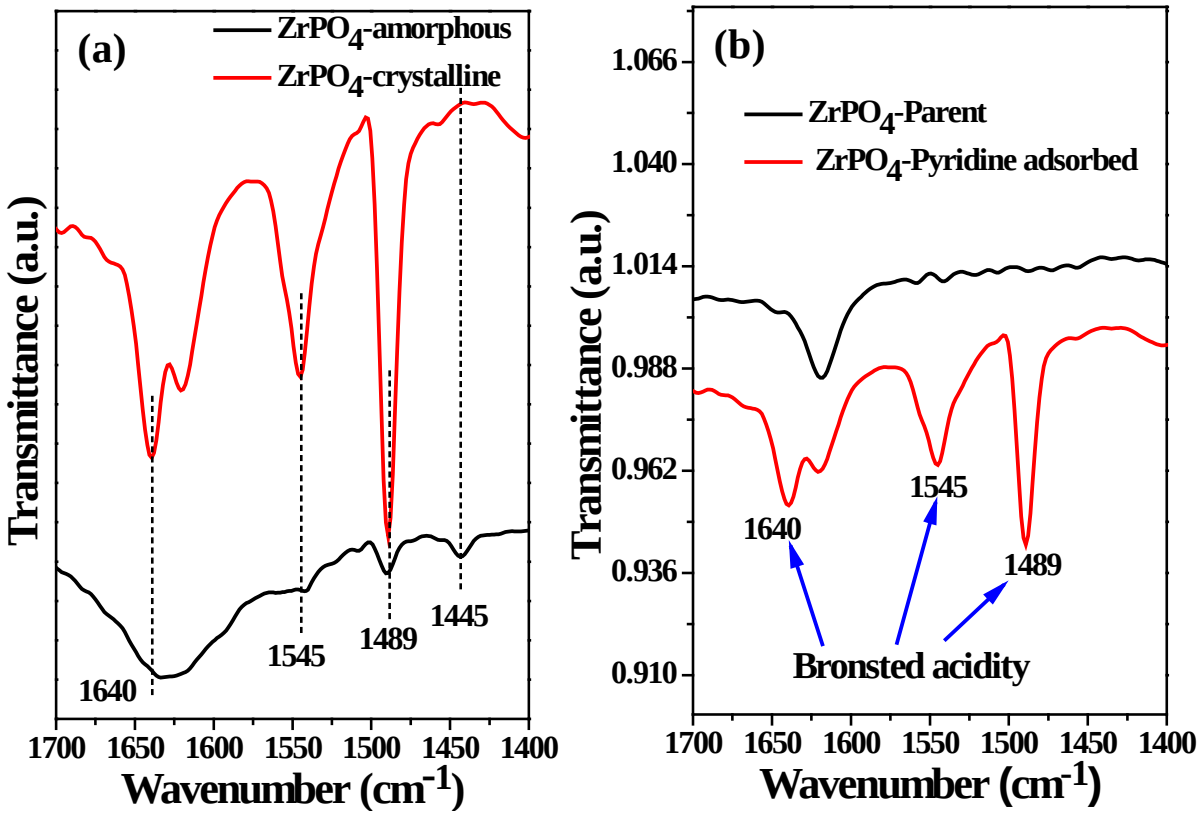

Figure S7. (a) Comparative pyridine FT-IR adsorbed spectra of crystalline and amorphous $ZrPO_4$ and (b) comparative FT-IR spectra of crystalline $ZrPO_4$ and pyridine adsorbed crystalline $ZrPO_4$,

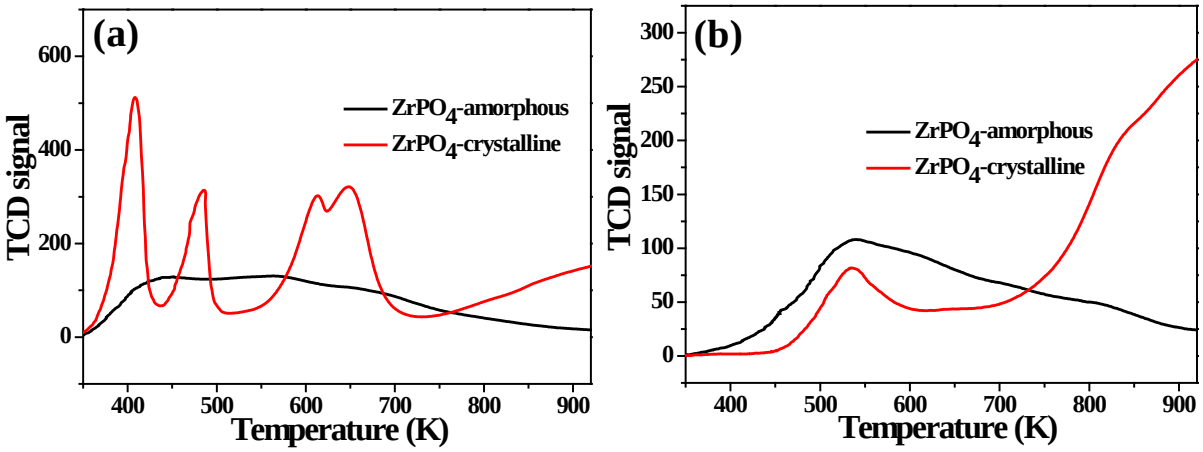

Figure S8. Comparative (a) NH_3-TPD and (b) CO_2-TPD of crystalline and amorphous $ZrPO_4$,

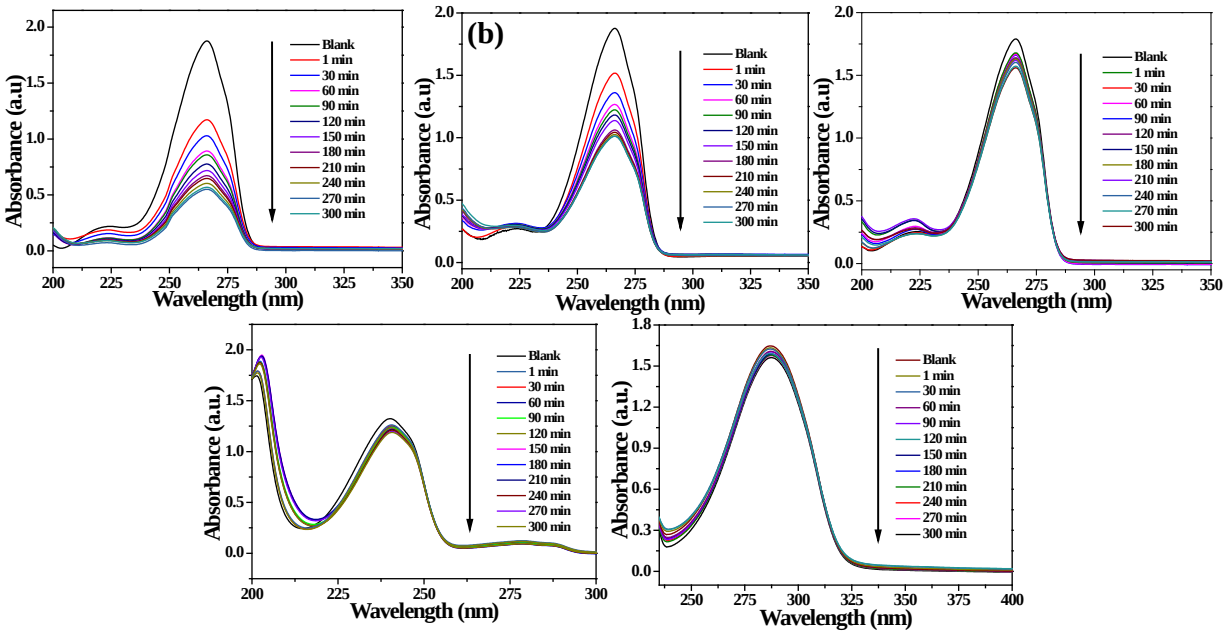

Figure S9. UV-visible spectra for the adsorption of FAL over (a) $ZrPO_4$, (b) $TiPO_4$, and (c) $SnPO_4$ and for the adsorption of (d) benzaldehyde and (e) cinnamaldehyde over $ZrPO_4$.

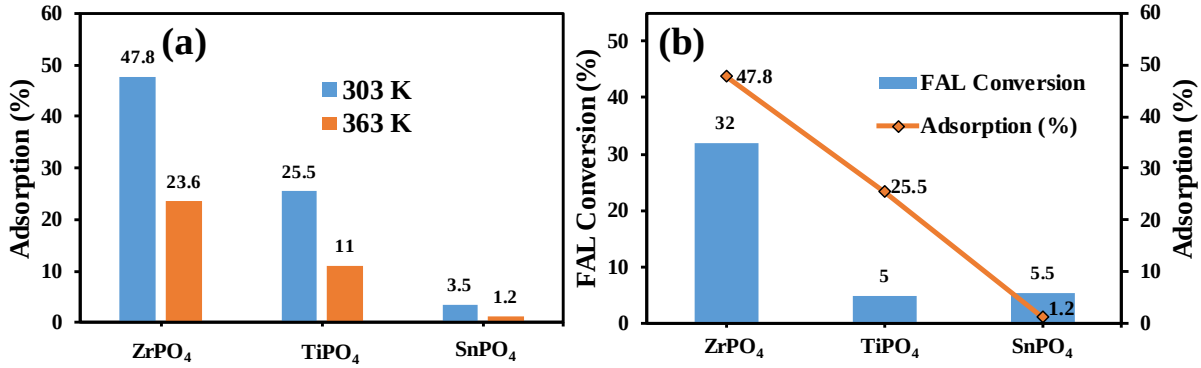

Figure S10. (a) Comparative adsorption of FAL over different metal phosphate at 303 K and 363 K from UV-visible measurement, (b) catalytic activity and adsorption data over different metal phosphates at 363 K.

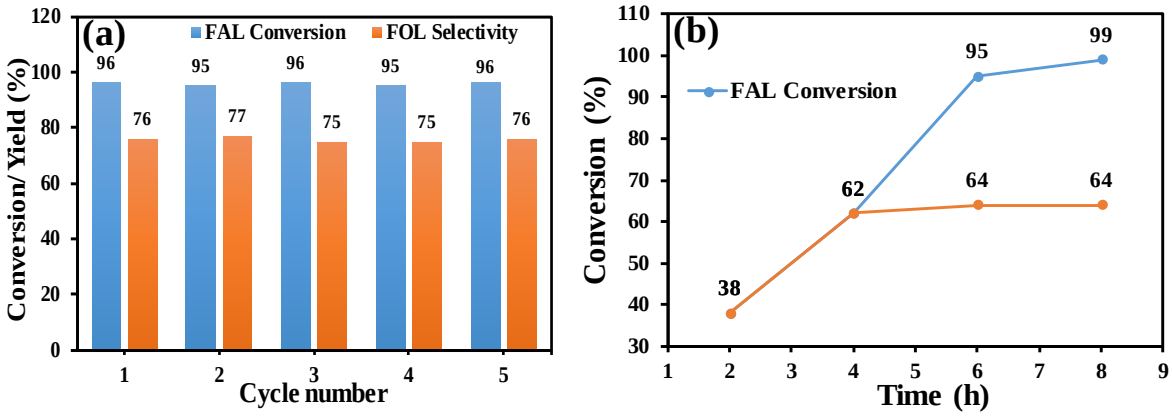

Figure S11. (a) Recyclability test of $ZrPO_4$ in the transfer hydrogenation of FAL to FOL using isopropanol [FAL (1mmol), $ZrPO_4$ (50 mg), 2-propanol (7 ml), temperature (393 K), and reaction time (6 h)] and (b) Hot-filtration test demonstrating the heterogeneity of the catalytic process.

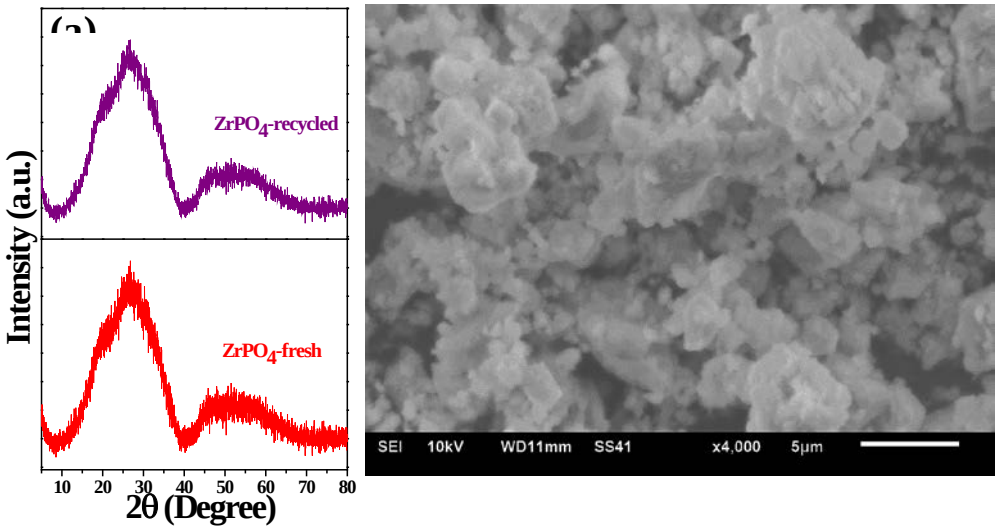

Figure S12. (a) XRD pattern and (b) SEM image of the recycled $ZrPO_4$ catalyst.

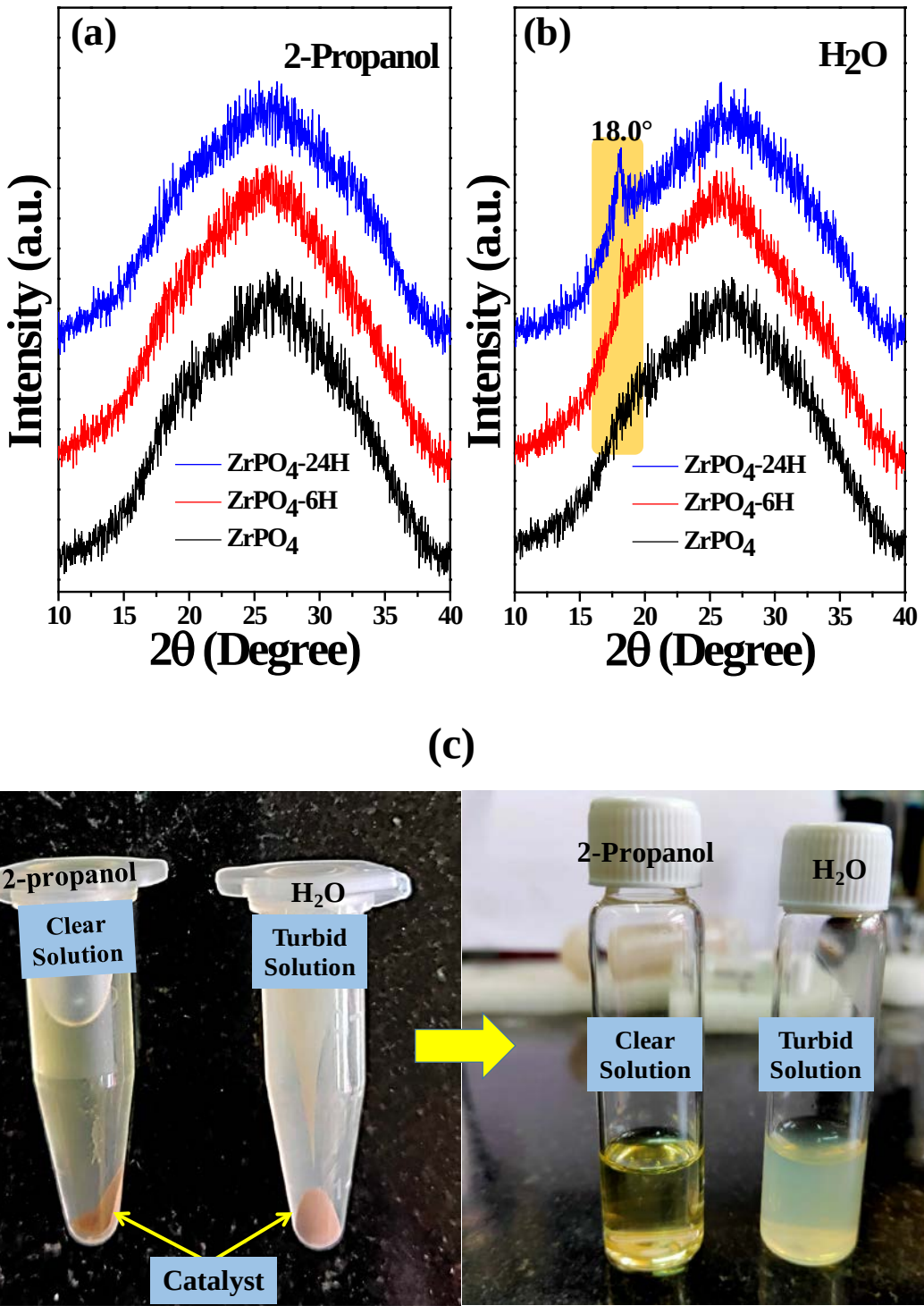

Figure S13. (a) Comparative XRD patterns of the fresh catalyst ($ZrPO_4$) and 2-propanol treated catalyst at 120 °C for 6 h and 24 h, (b) comparative XRD patterns of the fresh catalyst ($ZrPO_4$) and water treated catalyst at 120 °C for 6 h and 24 h, and (c) photographs demonstrating that the catalyst is stable in 2-propanol at 120 °C but leaches in water heated at 120 °C.

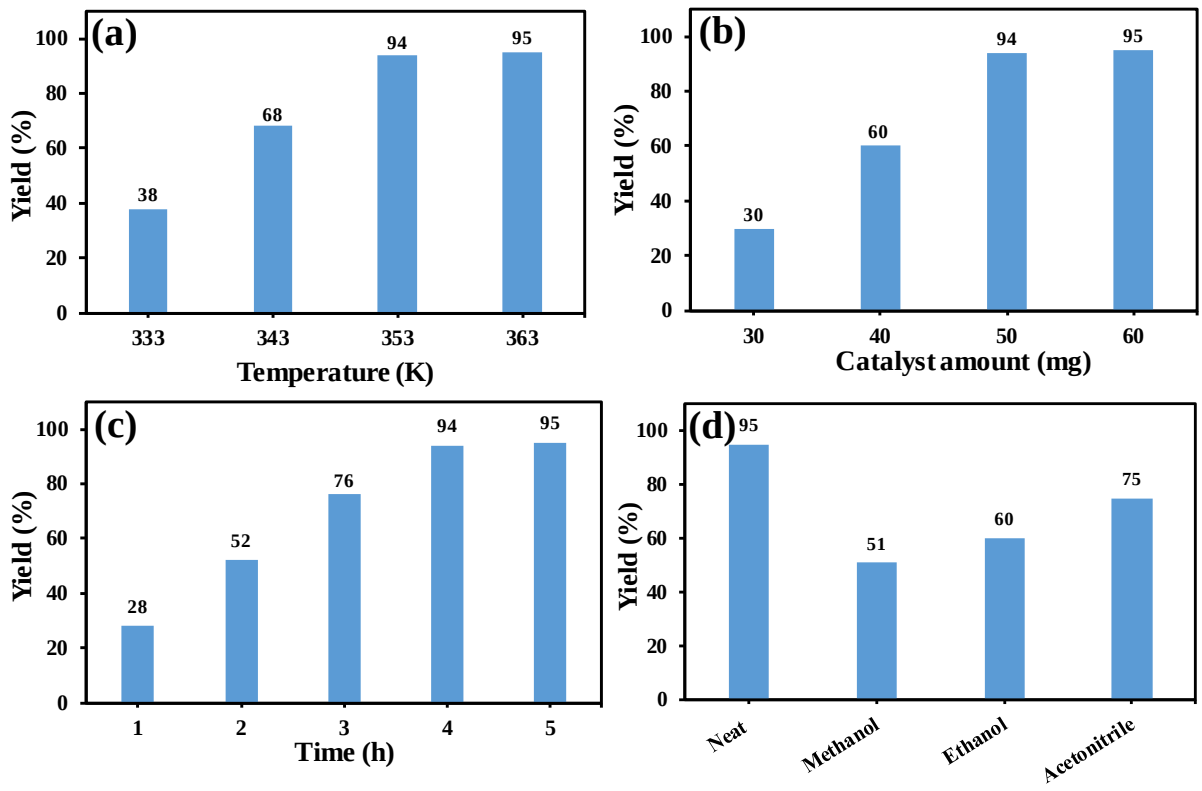

Figure S14. The optimization of reaction parameters for $ZrPO_4$ catalyzed Biginelli reaction. (a) Influence of temperature [FAL (2 mmol), acetylacetone (2 mmol), urea (3 mmol), $ZrPO_4$ (50 mg), solvent-free, time (4 h), and temperature (353 K)]; (b) Influence of catalyst amount [FAL (2 mmol), acetylacetone (2 mmol), urea (3 mmol), catalyst ($ZrPO_4$), time (4 h), solvent-free, and temperature (353 K)]; Influenc of time [FAL (2 mmol), acetylacetone (2 mmol), urea (3 mmol), $ZrPO_4$ (50 mg), solvent-free, and temperature (353 K).]; Influenc of solvent [FAL (2 mmol), acetylacetone (2 mmol), urea (3 mmol), catalyst $ZrPO_4$ (50 mg), time (4 h), and temperature (353 K).]

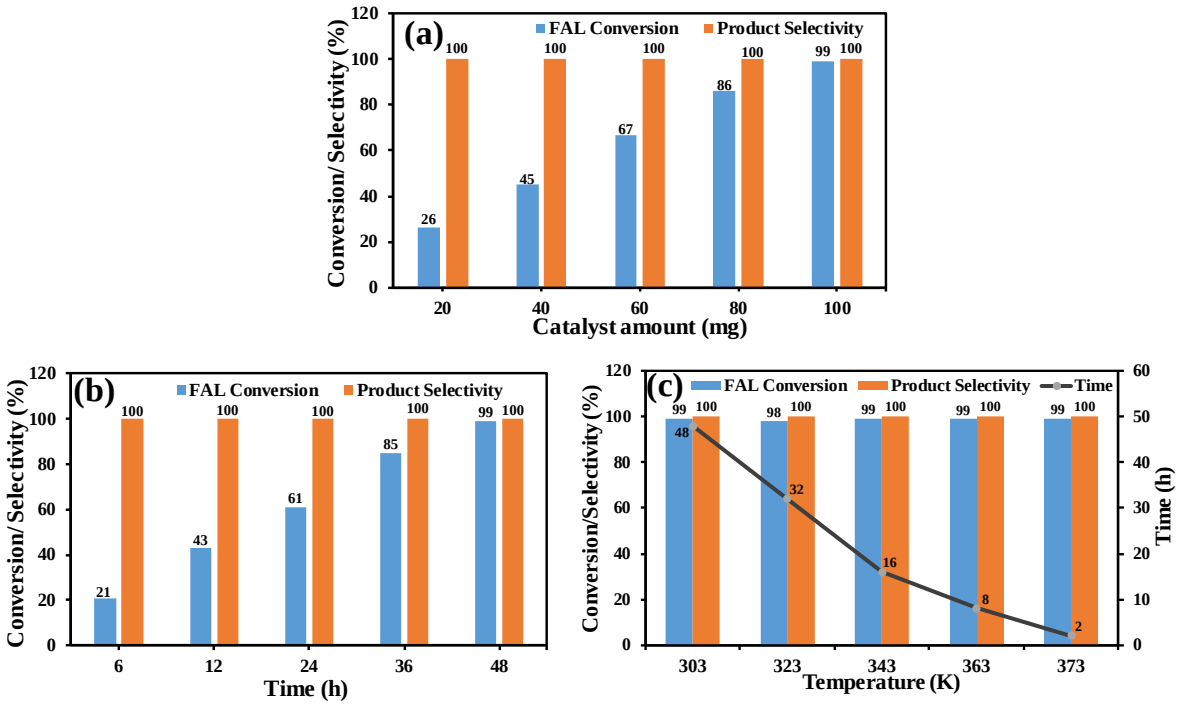

Figure S15. The optimization of reaction parameters for $ZrPO_4$ catalyzed Knoevenagel condensation between FF and malononitrile. (a) Influence of catalyst amount [FAL (1.7 mmol), malononitrile (1.7 mmol), catalyst ($ZrPO_4$), DCM (3 mL), temp. (303 K), and time (48 h)]; Influenc of time [FAL (1.7 mmol), malononitrile (1.7 mmol), $ZrPO_4$ (100 mg), DCM (3 mL)]; (c) variation in the catalytic activity at different temperature (vs time profile) to achieve the FAL conversion>98.

References

1 Dutta, A.; Patra, A. K.; Dutta, S.; Saha, B.; Bhaumik, A. Hierarchically Porous Titanium Phosphate Nanoparticles: An Efficient Solid Acid Catalyst for Microwave Assisted Conversion of Biomass and Carbohydrates into 5-Hydroxymethylfurfural. *J. Mater. Chem.* **2012**, *22*, 14094–14100. DOI: 10.1039/C2JM30623A.

2 Zhu, C.; Liu, Q.; Li, D.; Wang, H.; Zhang, C.; Cui, C.; Chen, L.; Cai, C.; Ma, L. Selective Hydrodeoxygenation of 5-Hydroxymethylfurfural to 2,5-Dimethylfuran over Ni Supported on Zirconium Phosphate Catalysts, *ACS Omega* **2018**, *3*, 7407-7417. DOI: 10.1021/acsomega.8b00609.

3 Gilkey, M. J.; Xu, B. Heterogeneous Catalytic Transfer Hydrogenation as an Effective Pathway in Biomass Upgrading. *ACS Catal.* **2016**, *6*, 1420–1436. DOI: 10.1021/acscatal.5b02171.

4 Fang, R.; Liu, H.; Luque, R.; Li, Y. Efficient and selective hydrogenation of biomass-derived furfural to cyclopentanone using Ru catalysts, *Green Chem.*, **2015**, *17*, 4183–4188. DOI: 10.1039/C5GC01462J.

5 Li, F.; France, L. J.; Cai, Z.; Li, Y.; Liu, S.; Lou, H.; Long, J.; Li, X. Catalytic Transfer Hydrogenation of Butyl Levulinate to γ-Valerolactone over Zirconium Phosphates with Adjustable Lewis and Brønsted Acid Sites. *Appl. Catal. B-Environ.* **2017**, *214*, 67–77. DOI: 10.1016/j.apcatb.2017.05.013.

6 Wang, Q.; Hou, W.; Li, S.; Xie, J.; Li, J.; Zhou, Y.; Wang, J. Hydrophilic Mesoporous Poly(Ionic Liquid)-Supported Au–Pd Alloy Nanoparticles towards Aerobic Oxidation of 5-Hydroxymethylfurfural to 2,5-Furandicarboxylic Acid under Mild Conditions. *Green Chem.* **2017**, *19*, 3820–3830. DOI: 10.1039/C7GC01116D.

7 Wang, F.; Zhang Z. Catalytic Transfer Hydrogenation of Furfural into Furfuryl Alcohol over Magnetic γ-Fe2O3@HAP Catalyst. *ACS Sustain. Chem. Eng.* **2017**, *5*, 942–947. DOI: 10.1021/acssuschemeng.6b02272.

8 He, J.; Li, H.; Riisager, A.; Yang, S. Catalytic Transfer Hydrogenation of Furfural to Furfuryl Alcohol with Recyclable Al–Zr@Fe Mixed Oxides. *ChemCatChem* **2018**, *10*, 430 – 438. DOI: 10.1002/cctc.201701266.

9 Li, J.; Liu, J.; Zhou, H.; Fu, Y. Catalytic Transfer Hydrogenation of Furfural to Furfuryl Alcohol over Nitrogen-Doped Carbon-Supported Iron Catalysts. *ChemSusChem* **2016**, *9*, 1339–1347. DOI: 10.1002/cssc.201600089.

10 Chen, H.; Ruan, H.; Lu, X.; Fu, J.; Langrish, T.; Lu, X. Efficient catalytic transfer

hydrogenation of furfural to furfuryl alcohol in near-critical isopropanol over Cu/MgO-Al_2O_3catalyst. *Mol. Catal.* **2018**, *445*, 94–101. DOI: 10.1016/j.mcat.2017.11.011.

11 Liu, C.; Xu, G.; Hu, A.; Xie, Y.; Wang, H. Porous Zirconium Hydroxyphosphonoacetate: Catalyst for Conversion of Furfural into Furfuryl Alcohol. *ChemistrySelect* **2019**, 4, 8000 –8006. DOI: 10.1002/slct.201901612.

12 Li, F.; Jiang, S.; Huang, J.; Wang, Y.; Lu, S.; Li, C. Catalytic transfer hydrogenation of furfural to furfuryl alcohol over a magnetic Fe_3O_4@C catalyst, *New J. Chem.* **2020**, 44, 478—486. DOI: 10.1039/C9NJ04698D.

13 Xu, G.; Liu, C.; Hu, A.; Xi, Y.; Wang, H.; Liu, X. Transfer hydrogenation of furfural to furfuryl alcohol over Keggin zirconium-heteropoly acid, *Mol. Catal.* **2019**, *475*, 110384. doi.org/10.1016/j.mcat.2019.04.013

14 Montes, V.; Miñambres, J. F.; Khalilov, A.N.; Boutonnet, M.; Marinas, J. M.; Urbano, F. J.; Maharramov, A.M.; Marinas, A. Chemoselective hydrogenation of furfural to furfuryl alcohol on ZrO_2 systems synthesized through the microemulsion method, *Catal. Today* **2018**, *306*, 89–95. DOI: 10.1016/j.cattod.2017.05.022.

15 Zhang, J.; Dong, K.; Luo, W.; Guan, H. Selective Transfer Hydrogenation of Furfural into Furfuryl Alcohol on Zr-Containing Catalysts Using Lower Alcohols as Hydrogen Donors, *ACS Omega* **2018**, *3*, 6206−6216. DOI: 10.1021/acsomega.8b00138.

16 Villaverde, M.M.; Garetto, T.F.; Marchi, A.J. Liquid-phase transfer hydrogenation of furfural to furfuryl alcohol on Cu–Mg–Al catalysts, *Catal. Commun.* **2015**, 58, 6–10. DOI: 10.1016/j.catcom.2014.08.021.

17 López-Asensio, R.; Cecilia, J.A.; Jiménez-Gómez, C.P.; García-Sancho, C.; Moreno-Tost, R.; Maireles-Torres, P.; Selective production of furfuryl alcohol from furfural by catalytic transfer hydrogenation over commercial aluminas, *Appl. Catal. A- Gen.* **2018**, *556*, 1–9. DOI: 10.1016/j.apcata.2018.02.022.

18 He, J.; Schill, L.; Yang, S.; Riisager, A. Catalytic Transfer Hydrogenation of Bio-Based Furfural with NiO Nanoparticles, *ACS Sustain. Chem. Eng.* **2018**, *6*, 17220−17229. DOI: 10.1021/acssuschemeng.8b04579.